Journal of Materials Chemistry B

PAPER

Facile scalable synthesis of highly monodisperse small silica nanoparticles using alkaline buffer solution and its application for efficient sentinel lymph node mapping

Received 00th January 20xx,
Accepted 00th January 20xx

DOI: 10.1039/x0xx00000x

www.rsc.org/

Bo Quan,[ae] Chaedong Lee,[a] Jung Sun Yoo,*[bcd] and Yuanzhe Piao*[ad]

Cancer nanomedicine involving nanotechnology-based drugs and *in vivo* imaging agents is an active field of nanoscience that provides new ways of enhancing therapeutic and diagnostic efficacy. Translating cancer nanomedicine mainly come from rational and scalable design of nanoparticles to achieve versatile properties including specific size because nanomaterials which their properties confer unique advantages can only optimize clinical impact. Here, facile scalable synthesis of highly monodisperse small silica nanoparticles was developed by screening various alkaline buffer solutions as catalysts. The size of silica nanoparticles ranging from 7 to 30 nm was finely controlled by varying the reaction temperature. Moderate sized silica nanoparticles in the range of 30 to 50 nm and large sized silica nanoparticles (>100 nm) were readily synthesized by in situ adding of tetraethylorthosilicate (TEOS) and applying the Stöber method in the reaction solution using small silica nanoparticles as the seeds, respectively. Having shown the ability to precisely synthesize size controlled silica nanoparticles with a process compatible with good manufacturing practices, we performed *in vivo* fluorescence imaging and immunofluorescent analysis of sentinel lymph node (SLN) with the synthesized nanoparticles having different sizes to investigate size effect for effective identification of SLN. The synthesized nanoparticles with a diameter of 12 nm showed effective SLN uptake within 10 min after intradermal injection both in noninvasive and in intraoperative imaging modes and were localized evenly inside the SLN. Whereas the 120 nm sized nanoparticles failed to identify SLN with noninvasive imaging at 10 min post-injection and distributed only in the medulla region not in the superficial cortex of the SLN. Taken together, a new facile scalable synthesis technique to achieve fine size controlling capability from very small silica nanoparticles (7 nm) was developed and it made possible to investigate the optimal size of nanoparticles for efficient SLN mapping which is still controversial.

Introduction

Silica has been considered as one of the valuable materials because of its plentiful supply in nature and useful properties, including photophysical inertness, chemical stability, and facile surface modification.[1, 2] Furthermore, silica is listed to be " generally recognized as safe" (GRAS) by the US Food and Drug Administration (FDA) due to its biocompatibility.[3] Owing to these characteristics, silica has been tried for a wide variety of applications, such as catalytic supports, molecular sieve, templates, and additives.[4-8] It is also beneficial for biomedical applications because silica is easy to use with physiologically relevant solutions. Among silica, silica-based nanospheres have attracted great interest for biological research and preclinical applications. For example, dye-doped silica nanoparticles have been studied as in vitro and *in vivo* imaging agents,[9-12] mesoporous silica nanoparticles have been used as drug- and DNA-delivery vessels,[13-18] and silica-based magnetic core-shell nanoparticles have been used for chemical sensor,[19] biocatalyst,[20] and magnetic resonance imaging (MRI) contrast agents.[21-23] Despite such vibrant applications with silica nanoparticles, development of key applications for clinical use is hampered by lack of large-scale, high-throughput synthesis methods with a precise size control. Therefore, the scalable synthesis of highly monodisperse fine silica nanoparticles is of key importance for successful biological applications and their translation into the clinic.

Controlled synthesis of monodisperse silica spheres with a diameter size range from 50 nm to 2 μm was developed by Stöber and coworkers in 1968.[24] Such synthetic method utilized hydrolysis and condensation of silicon alkoxides in an alcoholic solution in the presence of water and a base catalyst. However, it is difficult to synthesize small-sized silica nanoparticles (≤ 50 nm) using the Stöber method. Several synthetic methods have been reported in order to address this limitation of the Stöber method. Van Blaaderen et al. and Giesche et al. developed a seeded growth technique in the

[a] Program in Nano Science and Technology, Department of Transdisciplinary Studies, Graduate School of Convergence Science and Technology, Seoul National University, Seoul 08826, Republic of Korea. E-mail: parkat9@snu.ac.kr
[b] Smart Humanity Convergence Center, Program in Biomedical Radiation Sciences, Department of Transdisciplinary Studies, Graduate School of Convergence Science and Technology, Seoul National University, Seoul 08826, Republic of Korea.
[c] Department of Health Technology and Informatics, The Hong Kong Polytechnic University, Hong Kong SAR, E-mail: jungsun.yoo@polyu.edu.hk
[d] Advanced Institutes of Convergence Technology, Suwon 16229, Republic of Korea
[e] Department of Chemistry, Yanbian University, Yanji 133002, People's Republic of China.
† Electronic supplementary information (ESI) available:
See DOI: 10.1039/x0xx00000x

Stöber silica process to improve monodispersity and adjust the particle size.[25, 26] As an alternative route, monodisperse silica nanoparticles with 30-70 nm diameter were synthesized by using water-in-oil reverse microemulsion method.[27] However, these techniques also have some limitations, i.e., it is difficult to achieve large-scale synthesis and remove surfactants completely in the products.

Recently, there has been an effort to utilize basic amino acids (e.g., arginine and lysine) as a catalyst for the formation of monodisperse silica nanostructures.[28-30] Yokoi and co-workers reported the formation of monodisperse silica nanoparticles in the size range of 12 to 23 nm using L-lysine as a catalyst in place of ammonia.[31] Later, they demonstrated the formation mechanism of uniform-sized silica nanoparticles and the size of the silica nanoparticles could be controlled from 8 nm to 35 nm by varying the synthesis conditions and amounts of tetraethyl orthosilicate (TEOS).[32] Hartlen et al. reported the synthesis of highly monodisperse silica nanoparticles using an arginine as a catalyst and the as-prepared small silica nanoparticles as the seeds to grow into large-sized silica nanoparticles.[33] we developed a facile scalable synthesis of monodisperse silica nanoparticles using alkaline buffer solution. The size of monodisperse silica nanoparticles was finely controlled in a nanometer scale range (7-30 nm) and larger sized silica nanoparticles were synthesized by using regrowth approaches in reaction solution containing small sized silica nanoparticles acted as the seeds. We then investigated the formation mechanism of monodisperse silica nanoparticles and demonstrated that the process is more suitable for large-scale synthesis compared with previously reported methods.

Scalable synthesis of monodisperse silica nanoparticles from ultra-small size (7 nm) to large size (~hundreds nm) can provide a great benefit to study the effect of nanoparticles' size, which has been considered to play a major role in nanomedicine efficacy, *in vivo* pharmacokinetics, and other clinically relevant issues.[34] Here, we investigated size dependent imaging performance of silica nanoparticles for more efficient sentinel lymph node (SLN) mapping. The SLN concept, i.e., if the first lymph node to receive lymphatic drainage from a tumor site does not contain tumor cells, the tumor is not likely to have metastasized, and SLN biopsy have been a gold-standard for cancer management.[35] Recent focus has been given to the use of inorganic fluorescent nanoparticles as contrast agents for biomedical imaging such as pre- and intraoperative surgical guidance.[36-41] However, their optimal size range is still under debate. By utilizing precise size-controlled synthesis technique, we demonstrated that small silica nanoparticles (12 nm) can be more beneficial for rapid and sensitive identification of SLN compared to large silica nanoparticles (120 nm).

Experimental

Chemicals and materials

TEOS (98.0%), sodium hydroxide (NaOH 98.0%), cyclohexane (99.0%), ammonia solution (NH_4OH 28.0-30.0%), and ethanol (95.0%) were purchased from Samchun (Seoul, South Korea). Potassium chloride and ammonium chloride and were purchased from Sigma (St. Louis, MO, USA). Rhodamine B isothiocyanate (RITC), aminopropyltriethoxysilane (APTS 99.0%), cetyltrimethylammonium bromide (CTAB), and ethylenediaminetetracetic acid tetrasodium salt hydrate (EDTA 98%) were purchased from Aldrich (Milwaukee, WI, USA). Deionized water was prepared using a water purification system (UP90 model, Seoul, South Korea). All chemicals were used without further purification, unless otherwise specified.

Synthesis of small silica nanoparticles using alkaline buffer solutions

$NH_4Cl{\cdot}NH_3$ buffer solutions of pH 7.0, 8.0, 9.0, and 9.8 were prepared by adjusting 10 mM NH_4Cl with ammonia solution. A KCl·NaOH buffer solution was prepared by adjusting 10 mM KCl with 0.1 M NaOH solution to pH 11.8. An EDTA·NaOH buffer solution was prepared by adjusting 10 mM EDTA with 0.1 M NaOH solution to pH 8.0.

First, 40 mL of alkaline buffer solution was heated to a certain temperature and then a mixture of TEOS and cyclohexane was injected into the alkaline buffer solution. The volume ratio of TEOS and cyclohexane was changed from 1 to 2. The reaction mixture was vigorously stirred to mix the organic and inorganic layers well to form an emulsion for 24 h at the required temperatures. Finally, stirring was stopped and the solution was cooled to room temperature. After it had re-separated into an organic (top layer) and an aqueous layer (bottom layer), the aqueous layer that contained the silica nanoparticles was collected.

Large scale synthesis of small silica nanoparticles using alkaline buffer solutions

In a typical synthesis, 350 mL of $NH_4Cl{\cdot}NH_3$ buffer solution (pH = 9.0) was added to a 500 mL round-bottom flask and heated up to 60 °C. Once the temperature reached, a mixture of TEOS (100 mL) and cyclohexane (50 mL) was added to the flask and then the mixture solution was vigorously stirred into an emulsion for 24 h. After the solution was cooled to room temperature, the aqueous layer was collected.

In situ regrowth of silica nanoparticles

The as-prepared small-sized silica nanoparticles were regrown to obtain larger-sized silica nanoparticles (30-50 nm) in the same media. In a typical synthesis, a mixture of TEOS (3 mL) and cyclohexane (3 mL) was added to 40 mL of $NH_4Cl{\cdot}NH_3$ buffer (pH 9.0) solution with vigorous stirring at 70 °C for 24 h. Then, TEOS was added to the reaction mixture again and stirred for another 24 h. This step was repeated several times as necessary.

Regrowth of silica nanoparticles using the Stöber method

The small silica nanoparticles were used as the seeds in this regrowth process using the Stöber method. In a typical synthesis, 1 mL of small silica nanoparticles (concentration: 8 mg mL^{-1}) was diluted with a solution containing 90 mL of ethanol and 10 mL of water. After mixing, a certain amount of TEOS and 2.0 mL of ammonia solution were added to the mixture solution and stirred for 24 h at room temperature.

Synthesis of dye-doped silica nanoparticles

RITC-doped silica nanoparticles were also synthesized in this experiment. In a typical synthesis, 10 μL of APTS and 5.36 mg of RITC dye were added to 1.0 mL ethanol with stirring for 24 h to obtain RITC-APTS. 0.5 mL of RITC-ATPS solution was added to a mixture of 3 mL TEOS and 3 mL cyclohexane with shaking. The temperature of the buffer solution was heated to maintain a constant 60 °C and then a mixture of 3 mL TEOS and 3 mL cyclohexane was added with vigorous stirring for 24 h. The process was performed in a darkened room. The nanoparticles were collected by centrifugation with Amicon Ultra-4 Centrifugal Filter Units (50 kDa) from Millipore (Billerica, MA, USA) at 4,000 rpm for 20 min and washed several times.

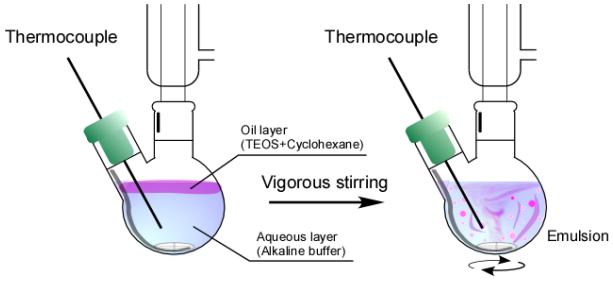

Scheme 1 Schematic model proposed for silica nanoparticle formation in an alkaline buffer solution. An organic/inorganic biphasic solution was turned into an emulsion with vigorous stirring.

Characterization of nanoparticles

Transmission electron microscopy (TEM) images were obtained from a JEOL EM-2010 microscope and the average size and standard deviation were measured by averaging diameters of more than 100 particles. The particle size distribution was analyzed using dynamic light scattering (DLS, ELSZ-2, Otsuka, Japan). Fluorescence spectra of dye-doped silica nanoparticles were obtained with a fluorescence spectrometer (FluoroMate FS–2, Scinco Co., Korea). The pH of mixture solution was measured using an Orion 3-star pH meter (Thermo Fisher Scientific, Waltham, MA, USA). The surface area of silica nanoparticles was analysed by N_2-adsorption/desorption isotherms by using the Brunauer–Emmett–Teller (BET) method. The pore size distribution were determined by using the Barrett–Joyner–Halenda model.

In vivo fluorescence imaging of lymph node

A male Balb/c nude mouse was purchased from the DooYeol Biotech. (Seoul, Korea) and their use was approved by the Institutional Animal Care and Use Committee of the Seoul National University. All animal experiments were carried out in accordance with the approved guidelines. A mouse was anaesthetized with intraperitoneal administration of zoletil (30 mg kg^{-1}), xylazine (5 mg kg^{-1}). The body temperature of the mouse was kept constant at 37 °C during all procedures. The nanoparticles with diameters of 12 nm and 120 nm [800 μg in 80 μL of saline] were intradermally injected in the left and right paws, respectively. *In vivo* fluorescence images of the mouse were obtained using a MVX10 imaging system (Olympus, Tokyo, Japan) after injection (Excitation: 550 ± 22.5 nm, Emission: 580 ± 30 nm). Imaging data were analyzed with Matlab software (MathWorks, Natick, MA, USA). The target-to-background ratio (TBR) of the sentinel lymph node (SLN) was determined as the ratio of the mean intensity calculated on the identified lymph node region divided by the one calculated in a similar area of surrounding fat and muscle tissue.

Immunofluorescence staining

After *in vivo* fluorescence imaging, the mouse was euthanized and the axillary lymph node was excised. After immediate *ex vivo* fluorescence imaging, the lymph node was embedded in a tissue-freezing medium (Triangle Biomedical Sciences, Durham, NC, USA), frozen, and consecutively cryo-sectioned in 8-µm segments. The tissue sections were thaw-mounted onto silane-coated microscope slides (Muto Pure Chemicals co., Tokyo, Japan), dried in an aeration room, and stored at -80 °C until use. For immunofluorescence staining, the tissue sections were rinsed with PBS and fixed with 4 % paraformaldehyde for 20 minutes at room temperature (RT). After an additional series of washing with PBS, the tissue sections were cleared with 3 % sodium deoxycholate solution for 2 hours at RT, blocked with 20 % normal goat serum in 1 % bovine serum albumin (BSA)-PBS for 2 h at 37 °C, incubated with the primary antibodies at 4 °C overnight (>17 hours). Specific antibodies against CD11b (1:200, MCA711G, AbD Serotec, Raleigh, NC, USA), F4/80 (1:100, MF48000, Life Technologies, Carlsbad, CA, USA), CD169 (1:200, MCA884, AbD Serotec, Raleigh, NC, USA), and B220 (1:150, 553084, BD Bioscience, Franklin Lakes, NJ, USA) were used on lymph node sections after dilution with 1 % BSA-PBS. Subsequently, the slides were rinsed three times with PBS and incubated with secondary antibody (1:400, Alexa Fluor 488 labelled, A11006, Life technologies, Carlsbad, CA, USA) at 4 °C for 2 hours. Then, they were washed with PBS several times, counterstained with Hoechst33342 and mounted with Pro-Long Gold antifade reagent (Life Technologies). The images of the immune-stained slides were captured with an A1 Rsi confocal microscope (Nikon, Tokyo, Japan).

Results and discussion

Synthetic scheme of silica nanoparticles

The monodisperse silica nanoparticles were easily synthesized using biphasic solution composed of cyclohexane as organic layer and alkaline buffer solution as aqueous layer and catalyst (Scheme 1, also see Fig. S1 in the Supporting information). The size of the silica nanoparticles was controlled by varying the reaction temperature. When the reaction temperature of alkaline buffer solution was 25 °C, 30 °C, 40 °C, 50 °C, 60 °C, and 70 °C in an $NH_4Cl{\cdot}NH_3$ buffer solution (pH 9.8), 7 nm, 9 nm, 13 nm, 17 nm, 22 nm, and 26 nm sized monodisperse silica nanoparticles were synthesized, respectively as shown in Fig. 1. We found that there was a linear correlation between the size of silica nanoparticles and the reaction temperature (Fig. 1G). Similar results were obtained when the pH of the $NH_4Cl{\cdot}NH_3$ buffer solution was changed to 9.0 (see Fig. S2 in the Supporting Information).

Optimization of synthetic conditions to produce uniform and monodisperse silica nanoparticles.

The formation of silica nanoparticles was also investigated by varying the pH value of the $NH_4Cl{\cdot}NH_3$ buffer solution. Buffers

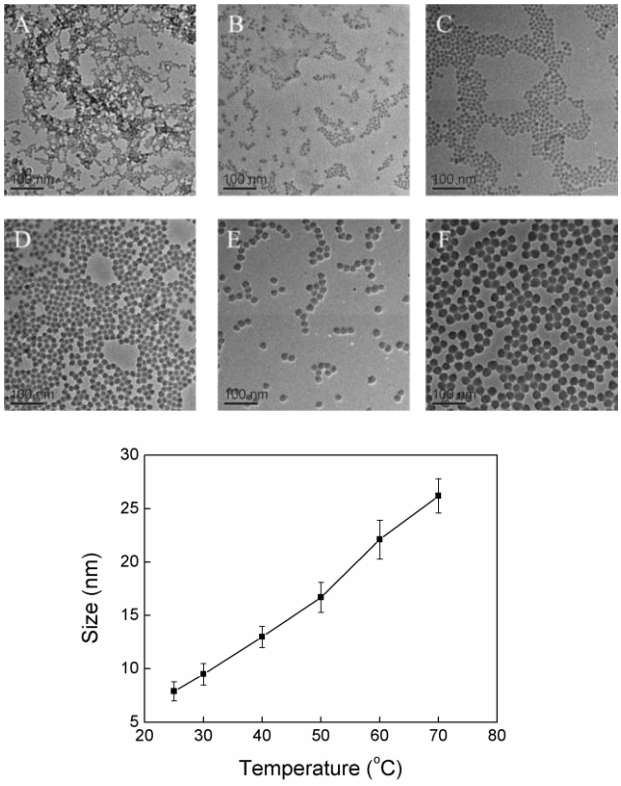

Fig. 1 Synthesis of silica nanoparticles using a $NH_4Cl{\cdot}NH_3$ buffer solution (pH = 9.8). TEM images of silica nanoparticles with particle diameters of (A) 7 nm, (B) 9 nm, (C) 13 nm, (D) 17 nm, (E) 22 nm, and (F) 26 nm. (G) Plot of the diameter of silica nanoparticles as temperature increases.

of pH 7.0, 8.0, 9.0, and 9.8 were prepared by adjusting 8 mM NH_4Cl with ammonia solution. According to Henderson-Hasselbalch equations, about 0.4%, 5%, 40%, and 78% of the buffer solution is in the form of NH_3. These buffer solutions were used to synthesize silica nanoparticles at 70 °C for 24 h. Monodisperse silica nanoparticles were successfully produced at pH 8.0, 9.0, and 9.8, but only a highly aggregated silica pieces were obtained at pH 7.0 of buffer solution (see Fig. S3 in the Supporting Information). Highly aggregated nanostructures were also produced at the range of the reaction temperature from 30 °C to 50 °C at pH 7.0 of buffer solution (see Fig. S4 in the Supporting Information).

It is well known that silica sphere formation is a result of hydrolysis of TEOS in basic solutions. Therefore, the pH of the buffer is an important factor that can define the fraction of the buffer agent formation. Roth et al. reported that small molecules, e.g., ethanolamine, 2-(dimethylamino) ethanethiol hydrochloride, 2-(ethylthio) ethylamine hydrochloride, cysteamine, propylamine, and 1-propanethiol were used as catalysts for hydrolysis, which maintained moderately stable pH over the course of the experiment.[42] In addition, neutral buffer (pH 7.0) alone does not significantly catalyze the hydrolysis. Yokoi et al.[31] and Davis et al.[28] reported that the formation of small silica nanoparticles can be achieved by using amino acids dissolved in an unbuffered, aqueous solution as catalysts. Amino acids are polyprotic acids that can donate or accept more than one proton.[43] Since the pKa's of carboxylic acid, ammonium, and substituents in amino acids (arginine) are 1.82, 8.99, and 12.1, respectively, under

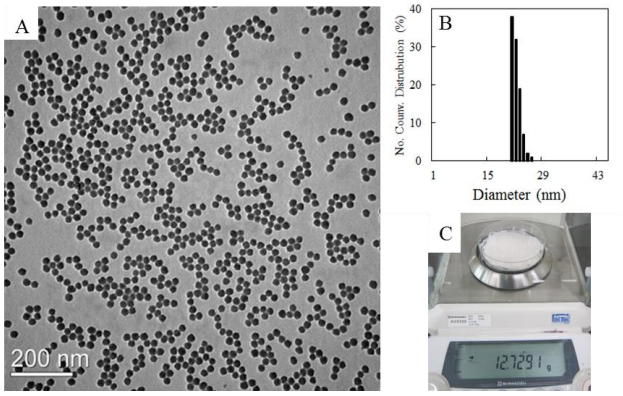

Fig. 2 (A) TEM image of monodisperse small silica nanoparticles in large scale synthesis. (B) Size distribution of small silica nanoparticles by DLS (mean diameter = 25 nm). (C) A photograph showing 12.7 g of silica nanoparticles in a single batch.

synthesis conditions (pH = 10), the major species is HArg (Scheme S1 in the Supporting Information). Because pH 10.0 is about one pH unit higher than pKa2 = 8.99, 90% of the arginine is in the HArg, and the second species is H_2Arg^+, which makes up about 10% of the arginine. Actually, the amino acid acted as a buffer agent in Yokoi et al. and Davis et al.'s processes. Amino acid molecules in the reaction solution can prevent interaction of protonated amino groups with the anionic silicates in order to control the size of silica nanoparticles.

In this study, a common alkaline buffer solution was used for TEOS hydrolysis. $NH_4Cl{\cdot}NH_3$ is a widely used buffer; the pKa of NH_4^+ is 9.24. In a synthesis condition (pH =9.0), the quotient $[NH_4^+]/[NH_3]$ is about 1.73. About 60% of the buffer solution is in the form of NH_4^+, and the remainder is in the form of NH_3. In this buffer process, the form of NH_3 catalyzes hydrolysis and condensation of TEOS. Furthermore, the buffer process can maintain a limited catalyst effect constantly and stably. Thus, the reaction using alkaline buffer solution can be finely controlled to produce a uniform silica nanostructure. In this process, TEOS was dissolved in the organic layer of cyclohexane and slowly released into the aqueous buffer layer, indicating a physical action to slow down the hydrolysis of TEOS.

Investigation with various alkaline buffer solutions

We found that the use of KCl·NaOH buffer (pH 11.8) and EDTA·NaOH buffer (pH 8.0) also led to the formation of similar small silica nanoparticles among various kinds of alkaline buffer solutions (see Figure S5 in the Supporting Information). These experiments demonstrated that alkaline buffer solutions can be used to synthesize small silica nanoparticles successfully. The previous research reported that, among 20 types of essential amino acids in protein, only L-lysine and L-arginine are useful to synthesize small silica nanoparticles.[31] When an amino acid is dissolved in solution, a fraction of the species was determined by the given pH. As we know, L-histidine, L-lysine, and L-arginine are categorized as basic amino acids in essential amino acids. Under basic conditions, the α-NH2 group, which is an effective catalytic form of amino acid, is predominant, except for L-histidine. Since the substituent (pKa= 5.97) of L-histidine is more acidic than the α-

NH_2 (pKa = 9.28) group, we estimated that this is the reason why only two amino acids can successfully lead to the formation of silica nanoparticles. The pH of other essential amino acids is low when they are dissolved in water. Thus, the fraction of effective catalytic form of the amino acid is too low to catalyse the hydrolysis reaction. A fraction of the α-NH_2 group can be increased with enough amount of high basic buffer solution. However, as we demonstrated, alkaline buffer solutions can produce silica nanoparticles without any catalyst additives.

Large-scale production of silica nanoparticles

The synthetic method developed here was scaled up 10-fold in a single batch to demonstrate large-scale production. For example, the amount of TEOS (0.44 mol) was mixed with cyclohexane and added into 350 mL of alkaline buffer solution, with a ratio almost similar to the 50 mL batch reaction. In previous research,[32, 33] the organic phase is developed on the top layer to control TEOS release. Hartlen et al. reported that vegetable oil can be used as a TEOS delivery medium to reduce pollution of oily waste from the large-scale process.[33] In this work, the organic layer and the inorganic layer were completely well-mixed with vigorous stirring to form an emulsion (Scheme 1; also see Figure S1 in the Supporting information). The amount of silica nanoparticles produced was 12.7 g (Fig. 2). DLS data show that the small silica nanoparticles had a mean diameter of 25 nm and had a narrow size distribution in water (Fig. 2B). The formation of an emulsion leads TEOS to release into the buffer solution more quickly. This shows that the alkaline buffer process is suitable for large-scale synthesis in real applications.

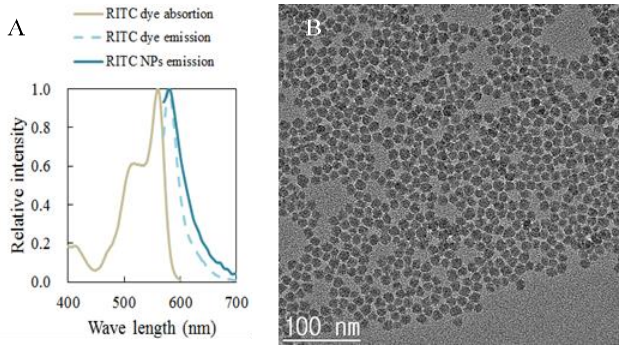

Fig. 3 (A) Normalized absorption, emission spectra of RITC dye, and emission spectra of RITC-doped silica nanoparticles. (B) TEM image of RITC-doped silica nanoparticles (12 nm).

N_2 adsorption/desorption isotherms and pore size distribution curve of small silica nanoparticles (20 nm) were analysed (Fig. S6). The small silica nanoparticles (20 nm) show a surface area

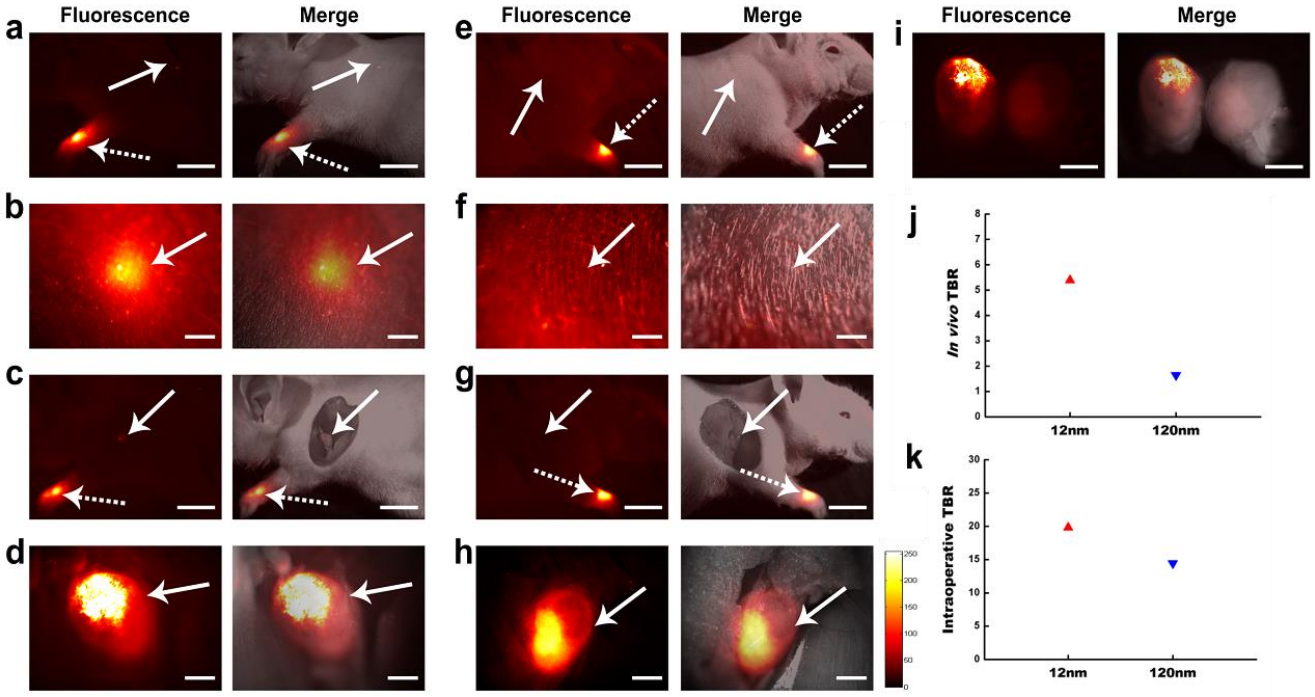

Fig. 4 *In vivo* sentinel lymph node (SLN) mapping with different sized fluorescent silica nanoparticles (NPs). (a-d) RITC-silica NPs with mean diameter of 12nm rapidly targets the SLN by fluorescence reflectance imaging. A strong fluorescence intensity was detected at the axillary lymph node (arrows in a and b) after 10 min of intradermal injection in the right paw (dotted arrows in a) of the mouse. Intraoperative inspection at 30min-postinjection confirmed the actual SLN (arrows in c and d) with vivid fluorescence signal. (e-h) Fluorescence reflectance images were also obtained after the left paw injection (dotted arrows in e) of 120 nm sized RITC-silica NPs under the identical experimental condition. Non-invasive imaging at 10 min-post-injection failed in identification of SLN (arrows in e and f). Only surgical imaging could discern the SLN (arrows in g and h) with marginal fluorescence intensity. (i) *Ex vivo* fluorescence images of dissected SLNs show different retention of NPs for the diameters of 12 nm (left) and 120 nm (right). Each set of images at identical magnification and exposure time have same overall contrast. The color lookup table applies to all fluorescence and merge images. (j-k) TBRs of the 12 nm and the 120 nm NPs injected mice were calculated using the *in vivo* (j) and intraoperative (k) images. The value of the TBR for 12 nm NPs injection was higher than that for 120 nm NPs injection. Scale bars, 4 mm in (a) and (e). Scale bars, 800 µm in (b) and (f). Scale bar, 2mm in (i).

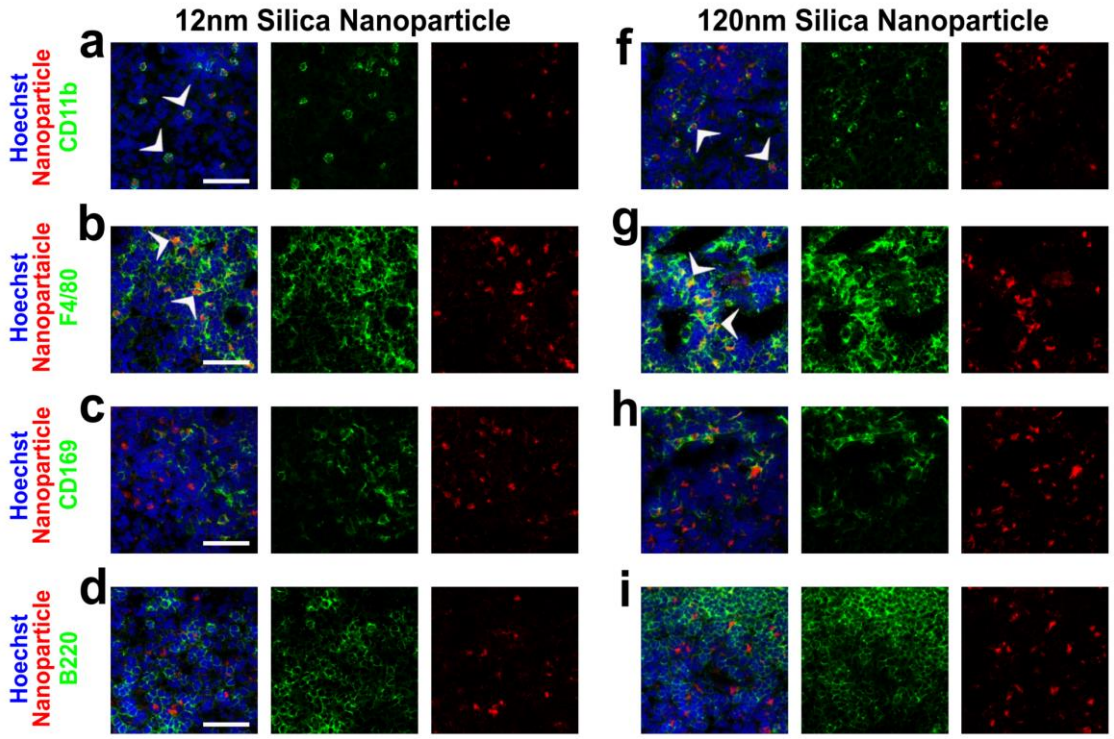

Fig. 5 Characterization of NP targeting and distribution in medulla of the SLN by immunofluorescence staining. Shown are confocal micrographs of frozen SLN sections from the mice injected with 12 nm (a-d) and 120 nm (f-i) RITC-silica NPs. The serial sections were stained with monoclonal antibodies (mAbs; green) against CD11b (a, f, monocytes/macrophages), F4/80 (b, g, medullary macrophages), CD169 (c, h, sub-capsular sinus macrophages), and B220 (d, i, B lymphocytes). No significant difference of NP deposit (red) for 12 nm and 120 nm was observed in lymph node medulla. All sections were counterstained with Hoechst 33342 for nuclei identification (blue). Arrowheads denote representative co-expressed cells with mAb and nanoparticles. Scale bars, 50 μm.

of 280.79 m^2 g^{-1} with the pore volume of 0.45 cm^3 g^{-1}. Our previous work has reported that silica nanoparticles with diameter size of 100 nm showed a surface area of 38 m^2 g^{-1}, which is much lower than small-sized silica nanoparticles.[8] No voids were observed in these silica nanoparticles even by high-magnification TEM (Fig S7). The pore size distribution curve of silica nanoparticles exhibited several peaks (5 nm, 43 nm and 92 nm, respectively, Fig. S6B). The results suggest that the pores are interstitial pores of the dried nonporous silica NPs agglomerates.

Synthesis of large sized silica nanoparticles

We showed that the size of the silica nanoparticles can be controlled by varying reaction temperature. In addition, an in situ regrowth approach was utilized to further control the size of silica nanoparticles up to a few hundred nm. After seed formation using alkaline buffer solutions, highly monodisperse silica nanoparticles of a desired size can be conveniently prepared by in situ adding TEOS to the reaction media. It revealed that 35 nm of silica nanoparticles were grown to 46 nm and 51 nm by adding 3 mL of TEOS once and twice, respectively (Fig. S5).

The regrowth process using the Stöber method is suitable for the synthesis of large-size silica nanoparticles.[18, 26, 33] In this work, 25 nm silica seed nanoparticles were re-dispersed in 100 mL of ethanol/H2O (9/1, v/v) at room temperature. Silica nanoparticles were grown to 100 nm and 150 nm by adding 0.5 mL and 1.0 mL of TEOS, respectively (Fig. S9). The size can be easily controlled by varying the ratio of TEOS, ethanol, and ammonia.

Synthesis of fluorescent silica nanoparticles

Recently, the FDA approved dye-doped silica nanoparticles (C-dots) for the first Investigational New Drug (IND) application for targeted molecular imaging of cancer.[1, 10, 44-48] Thus, it is highly required to improve the developed synthetic technique to produce dye-doped silica nanoparticles for broad biomedical applications. Table S1 summarizes previous research for development of dye doped silica nanoparticles. We selected RITC dye, which is a commonly used organic fluorophore in biological research. Fig. 3A and B show that RITC dye-doped silica nanoparticles with a size of 12 nm were well produced, and they had the same emission wavelength with RITC dye (peak at 595 nm) when they were excited at 555 nm. These results demonstrate that dye-doped silica nanoparticles could be synthesized by using alkaline buffer solutions successfully. We believe that the alkaline buffer process will be a useful approach to developing the C-dots.

***In vivo* SLN mapping using different sized silica nanoparticles**

Recently, inorganic fluorescent nanoparticles have emerged as promising alternatives for sensitive and more efficient localization of SLN, i.e., the first draining lymph node from primary tumor providing diagnostic information for metastasis. However, the preferred range for rapid lymphatic uptake and

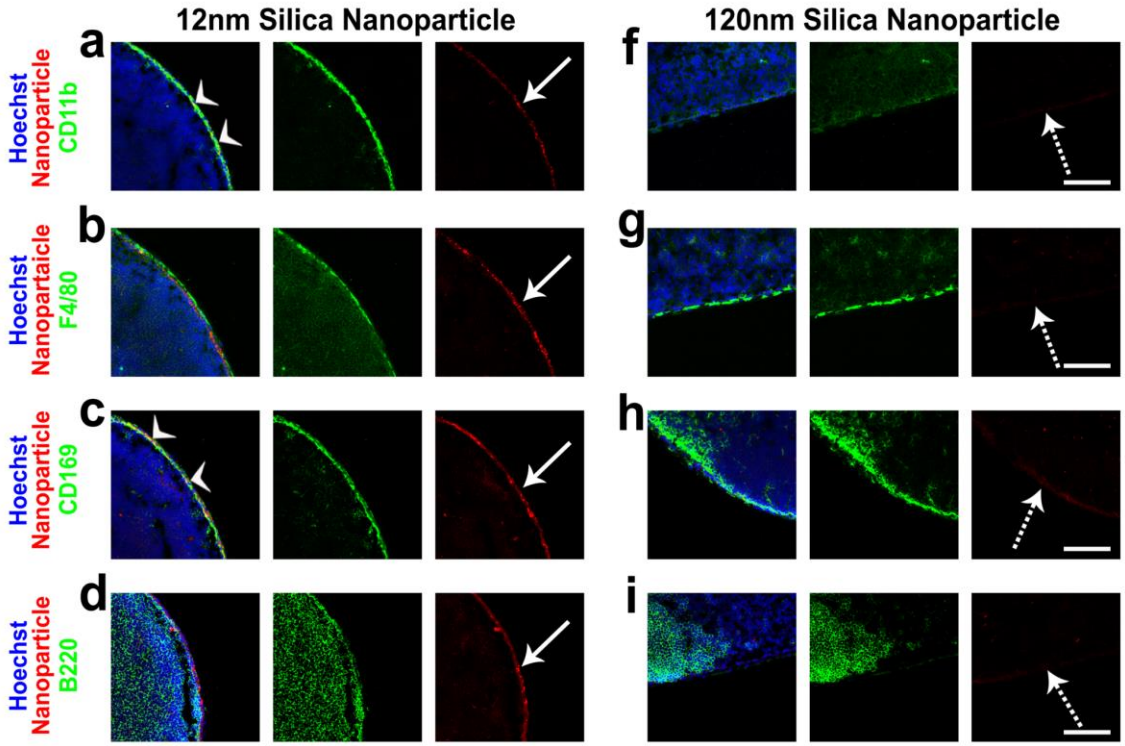

Fig. 6 Characterization of NP targeting and distribution in superficial cortex of the SLN by immunofluorescence staining. Shown are confocal micrographs of frozen SLN sections from the mice injected with 12 nm (a-d) and 120 nm (f-i) RITC-silica NPs. The serial sections were stained with monoclonal antibodies (mAbs; green) against CD11b (a, f, monocytes/macrophages), F4/80 (b, g, medullary macrophages), CD169 (c, h, sub-capsular sinus macrophages), and B220 (d, i, B lymphocytes). All sections were counterstained with Hoechst33342 for nuclei identification (blue). Sub-capsular sinus shows strong uptake for 12 nm sized NPs (red, arrows) by binding with macrophages, but no uptake for 120 nm sized NPs (dotted arrows). Arrowheads denote representative co-expressed cells with mAb and nanoparticles. Scale bars, 100

the optimal size for effective and accurate identification of SLNs are still under debate. Owing to the capability of the size-controlled synthesis, we could explore the size dependent SLN mapping performance with RITC-doped 12 nm and 120 nm sized nanoparticles (Fig. S10). After intradermal injection in the lymphatic-rich front paw of mice, each nanoparticle entered the lymphatic collecting vessels and migrated into axillary nodes (SLN) that could be detected by *in vivo* fluorescence imaging (Fig. 4). The 12 nm sized nanoparticles showed a strong fluorescence intensity in the SLN after 10 min post-injection with non-invasive imaging (Fig. 4a and b), however the signal of 120 nm sized nanoparticles was not detected without skin incision (Fig. 4e and f). Intraoperative inspection at 30 min post-injection confirmed the SLN both with 12 nm and 120 nm nanoparticles' imaging (Fig. 4c-d and 4g-h), but showed different target-to-background ratio (TBR)s, i.e., 19.83 and 14.44, respectively (Fig. 4k). Overall, the 12 nm sized nanoparticles demonstrated superior imaging performance compared to the 120 nm sized nanoparticles.

Localization and characterization of nanoparticles within the SLN

Having shown the better capability to detect the SLN with the 12 nm sized nanoparticles, we proceeded to verify the nanoparticle deposit with cellular level by immunofluorescence staining. Using fluorescent microscopic analysis of nanoparticles' signal and several markers which are specific for lymph-node-consisting cells, we were able to identify the characteristics of the nanoparticles' localization at cellular and tissue levels (Fig. 5 and 6). As shown in Fig. 5, no significant difference of nanoparticles' deposit for 12 nm and 120 nm was observed in lymph node medulla region. Whereas, in superficial cortex of the SLN, strong uptake for 12 nm sized nanoparticles was shown, but no uptake for 120 nm sized nanoparticles (Fig. 6). The silica nanoparticles with a diameter of 12 nm exhibited rapid uptake into the lymphatic system owing to their innate lymphotropic property and distributed evenly inside all area of lymph node. On the other hands, the 120 nm sized silica nanoparticles showed relatively slow uptake into the lymphatic system and remained in the medulla where afferent lymphatic vessels are connected. Presumably, such difference in cellular and tissue level localization resulted in different *in vivo* imaging performance. Both nanoparticles localized in the scattered large cells which expressed macrophage markers, including CD11b, F4/80 in medulla, CD169 in sub-capsular sinus. The nanoparticles' signal, however, did not co-localize with B220+ follicular B lymphocytes.

Conclusions

We demonstrated a facile scalable method for the size-controlled synthesis of monodisperse small silica nanoparticles

by using an alkaline buffer solution acted as a solvent and catalyst and showcased its potential to study size effect in biomedical application with nanoparticles by investigation of optimal size of silica nanoparticles for efficient sentinel lymph node mapping. The result shows that various alkaline buffer solutions can catalyze hydrolysis and condensation of TEOS, in a buffer region, to synthesize monodisperse silica nanoparticles. The size of monodisperse silica nanoparticles were easily controlled in the range of 7 nm to 30 nm by varying reaction temperature. Furthermore, the in situ regrowth and the Stöber regrowth approach were utilized to further produce larger sized silica nanoparticles from 30 nm to 150 nm. This synthetic approach is a convenient process for large-scale production up to 10-fold and the formation of dye-doped silica nanoparticles by simply adding dyes in the same process. The developed size controllable synthesis technique enabled to investigate the magnitude of optimal size of silica nanoparticles for efficient SLN mapping which is a controversial issue in cancer research. We believe that the presented synthetic approach can provide a powerful tool to advance nanotechnology to treat and image various diseases including cancer by enabling reliable investigation to find preferred size range of nanoparticles.

Acknowledgements

This research was supported by Basic Science Research Program through the National Research Foundation of Korea (NRF) funded by the Ministry of Education (NRF-2015R1D1A1A01060398) and by the Ministry of Science, ICT and Future Planning (2014R1A2A1A11053420), and the grant no. 13-2015-013 from the SNUBH Research Fund. This work was also supported under the framework of international cooperation program managed by National Research Foundation of Korea (NRF-2015K2A2A2002209) and by the Center for Integrated Smart Sensors funded by the Ministry of Science, ICT and Future Planning, Republic of Korea, as Global Frontier Project (CISS-012M3A6A6054186). This research was also supported by the National Natural Science Foundation of China (grant no. 21601152).

Notes and references

1. S. Bonacchi, D. Genovese, R. Juris, M. Montalti, L. Prodi, E. Rampazzo and N. Zaccheroni, *Angewandte Chemie International Edition*, 2011, **50**, 4056-4066.
2. J. E. Lee, N. Lee, T. Kim, J. Kim and T. Hyeon, *Accounts of Chemical Research*, 2011, **44**, 893-902.
3. Y. Piao, A. Burns, J. Kim, U. Wiesner and T. Hyeon, *Advanced Functional Materials*, 2008, **18**, 3745-3758.
4. Y. Wan, H. Wang, Q. Zhao, M. Klingstedt, O. Terasaki and D. Zhao, *Journal of the American Chemical Society*, 2009, **131**, 4541-4550.
5. C. Kresge, M. Leonowicz, W. Roth, J. Vartuli and J. Beck, *nature*, 1992, **359**, 710-712.
6. J. E. Schmidt, M. W. Deem and M. E. Davis, *Angewandte Chemie International Edition*, 2014, **53**, 8372-8374.
7. S.-H. Yu, B. Quan, A. Jin, K.-S. Lee, S. H. Kang, K. Kang, Y. Piao and Y.-E. Sung, *ACS Applied Materials & Interfaces*, 2015, **7**, 25725-25732.
8. B. Quan, G.-E. Nam, H. J. Choi and Y. Piao, *Chemistry – An Asian Journal*, 2013, **8**, 765-770.
9. S. Santra, P. Zhang, K. Wang, R. Tapec and W. Tan, *Analytical Chemistry*, 2001, **73**, 4988-4993.
10. A. A. Burns, J. Vider, H. Ow, E. Herz, O. Penate-Medina, M. Baumgart, S. M. Larson, U. Wiesner and M. Bradbury, *Nano letters*, 2008, **9**, 442-448.
11. M. Montalti, L. Prodi, E. Rampazzo and N. Zaccheroni, *Chemical Society Reviews*, 2014, **43**, 4243-4268.
12. B. Quan, K. Choi, Y.-H. Kim, K. W. Kang and D. S. Chung, *Talanta*, 2012, **99**, 387-393.
13. B. G. Trewyn, I. I. Slowing, S. Giri, H.-T. Chen and V. S.-Y. Lin, *Accounts of chemical research*, 2007, **40**, 846-853.
14. I. I. Slowing, B. G. Trewyn, S. Giri and V. Y. Lin, *Advanced Functional Materials*, 2007, **17**, 1225-1236.
15. Y. Hoshikawa, H. Yabe, A. Nomura, T. Yamaki, A. Shimojima and T. Okubo, *Chemistry of Materials*, 2009, **22**, 12-14.
16. L. Han, H. Wei, B. Tu and D. Zhao, *Chemical Communications*, 2011, **47**, 8536-8538.
17. M. P. Conley, C. Copéret and C. Thieuleux, *ACS Catalysis*, 2014, **4**, 1458-1469.
18. X. Li, Q. He and J. Shi, *ACS Nano*, 2014, **8**, 1309-1320.
19. A. Burns, P. Sengupta, T. Zedayko, B. Baird and U. Wiesner, *Small*, 2006, **2**, 723-726.
20. J. Lee, Y. Lee, J. K. Youn, H. B. Na, T. Yu, H. Kim, S. M. Lee, Y. M. Koo, J. H. Kwak and H. G. Park, *Small*, 2008, **4**, 143-152.
21. T. Kim, E. Momin, J. Choi, K. Yuan, H. Zaidi, J. Kim, M. Park, N. Lee, M. T. McMahon and A. Quinones-Hinojosa, *Journal of the American Chemical Society*, 2011, **133**, 2955-2961.
22. T. Zhang, J. Ge, Y. Hu, Q. Zhang, S. Aloni and Y. Yin, *Angewandte Chemie*, 2008, **120**, 5890-5895.
23. Y. Wang and H. Gu, *Advanced Materials*, 2015, **27**, 576-585.
24. W. Stöber, A. Fink and E. Bohn, *Journal of colloid and interface science*, 1968, **26**, 62-69.
25. A. Van Blaaderen, J. Van Geest and A. Vrij, *Journal of colloid and interface science*, 1992, **154**, 481-501.
26. H. Giesche, *Journal of the European Ceramic Society*, 1994, **14**, 205-214.
27. F. Arriagada and K. Osseo-Asare, *Journal of colloid and interface science*, 1999, **211**, 210-220.
28. T. M. Davis, M. A. Snyder, J. E. Krohn and M. Tsapatsis, *Chemistry of Materials*, 2006, **18**, 5814-5816.
29. M. A. Snyder, J. A. Lee, T. M. Davis, L. Scriven and M. Tsapatsis, *Langmuir*, 2007, **23**, 9924-9928.
30. T. Yokoi, T. Karouji, S. Ohta, J. N. Kondo and T. Tatsumi, *Chemistry of Materials*, 2010, **22**, 3900-3908.
31. T. Yokoi, Y. Sakamoto, O. Terasaki, Y. Kubota, T. Okubo and T. Tatsumi, *Journal of the American Chemical Society*, 2006, **128**, 13664-13665.
32. T. Yokoi, J. Wakabayashi, Y. Otsuka, W. Fan, M. Iwama, R. Watanabe, K. Aramaki, A. Shimojima, T. Tatsumi and T. Okubo, *Chemistry of Materials*, 2009, **21**, 3719-3729.
33. K. D. Hartlen, A. P. Athanasopoulos and V. Kitaev, *Langmuir*, 2008, **24**, 1714-1720.
34. E. K.-H. Chow and D. Ho, *Science translational medicine*, 2013, **5**, 216rv214-216rv214.
35. R. J. Bleicher and E. R. Sigurdson, *Current problems in cancer*, 2012, **36**, 263-291.

36. S. Kim, Y. T. Lim, E. G. Soltesz, A. M. De Grand, J. Lee, A. Nakayama, J. A. Parker, T. Mihaljevic, R. G. Laurence and D. M. Dor, *Nature biotechnology*, 2004, **22**, 93-97.
37. F. Erogbogbo, K.-T. Yong, I. Roy, R. Hu, W.-C. Law, W. Zhao, H. Ding, F. Wu, R. Kumar and M. T. Swihart, *ACS nano*, 2010, **5**, 413-423.
38. T. Pons, E. Pic, N. Lequeux, E. Cassette, L. Bezdetnaya, F. Guillemin, F. Marchal and B. Dubertret, *ACS nano*, 2010, **4**, 2531-2538.
39. Z. Liu, E. Ju, J. Liu, Y. Du, Z. Li, Q. Yuan, J. Ren and X. Qu, *Biomaterials*, 2013, **34**, 7444-7452.
40. Z. Liu, Z. Li, J. Liu, S. Gu, Q. Yuan, J. Ren and X. Qu, *Biomaterials*, 2012, **33**, 6748-6757.
41. Z. Liu, F. Pu, S. Huang, Q. Yuan, J. Ren and X. Qu, *Biomaterials*, 2013, **34**, 1712-1721.
42. K. M. Roth, Y. Zhou, W. Yang and D. E. Morse, *Journal of the American Chemical Society*, 2005, **127**, 325-330.
43. D. C. Harris, *Quantitative chemical analysis*, Macmillan, 2010.
44. H. Ow, D. R. Larson, M. Srivastava, B. A. Baird, W. W. Webb and U. Wiesner, *Nano letters*, 2005, **5**, 113-117.
45. J. E. Fuller, G. T. Zugates, L. S. Ferreira, H. S. Ow, N. N. Nguyen, U. B. Wiesner and R. S. Langer, *Biomaterials*, 2008, **29**, 1526-1532.
46. E. Herz, H. Ow, D. Bonner, A. Burns and U. Wiesner, *Journal of Materials Chemistry*, 2009, **19**, 6341-6347.
47. M. Benezra, O. Penate-Medina, P. B. Zanzonico, D. Schaer, H. Ow, A. Burns, E. DeStanchina, V. Longo, E. Herz and S. Iyer, *The Journal of clinical investigation*, 2011, **121**, 2768-2780.
48. R. Friedman, *Journal of the National Cancer Institute*, 2011, **103**, 1428-1429.